

Nanoscale

Accepted Manuscript



This is an *Accepted Manuscript*, which has been through the Royal Society of Chemistry peer review process and has been accepted for publication.

Accepted Manuscripts are published online shortly after acceptance, before technical editing, formatting and proof reading. Using this free service, authors can make their results available to the community, in citable form, before we publish the edited article. We will replace this *Accepted Manuscript* with the edited and formatted *Advance Article* as soon as it is available.

You can find more information about *Accepted Manuscripts* in the [Information for Authors](#).

Please note that technical editing may introduce minor changes to the text and/or graphics, which may alter content. The journal's standard [Terms & Conditions](#) and the [Ethical guidelines](#) still apply. In no event shall the Royal Society of Chemistry be held responsible for any errors or omissions in this *Accepted Manuscript* or any consequences arising from the use of any information it contains.

INVITED REVIEW

Color Generation via Subwavelength Plasmonic Nanostructures

Cite this: DOI:

Yinghong Gu^a, Lei Zhang^a, Joel K.W. Yang^{b,c}, Swee Ping Yeo^a and Cheng-Wei Qiu^a

Received 00th xxx 2015,

Accepted 00th xxx 2015

DOI:

www.rsc.org/

Recent developments in color filtering and display technologies focus predominantly on high resolution, color vibrancy, high efficiency, and slim dimensions. To achieve these goals, metallic nanostructures have attracted extensive research interest due to their abilities to manipulate the properties of light through surface plasmon resonances. In this paper, we will review recent representative developments in plasmonic color engineering at the nanoscale using subwavelength nanostructures, demonstrating their great potential in high-resolution and high-fidelity color rendering, spectral filtering applications, holography, three-dimensional stereoscopic imaging, etc.

Key words: color filtering, imaging, surface plasmon, plasmonic nanostructure.

1. Introduction

In nature, colors are mainly produced by the light scattering or partial absorption of materials. Color displays such as emissive liquid-crystal displays employ pigment-based color filters to absorb the complementary colors to produce the red, green, and blue channels^{1, 2, 3}. With the drive towards higher-resolution imaging and displays, new innovations are needed to achieve higher resolution, lower power consumption, higher compactness, and also color tunability in devices. The highest possible resolution in theory for color display and imaging is set by the diffraction limit of the accompanying optics⁴, which is ~250-nm-pitch for imaging through high numerical-aperture objectives with visible light. However, the resolution of existing pigment-based color printing can just reach the level of ten micrometers, still 1 or 2 orders away from this target.

Alternatively, colors can also be generated by structure engineering, such as diffraction optic devices, photonic crystals, and plasmonic structures. Some naturally occurring photonic structures generate the colorful appearance of some types of insects, birds and aquatic animals^{5–12}, usually with the combined effects of thin film/multilayer interferences, grating diffraction, photonic crystals

and light scattering. An example of natural structural color is that of butterfly wings, which has been widely investigated, and reproduced through nanostructures fabricated in labs^{7–12}. It has been demonstrated that this structural color effect based on photonic crystals, nanowire arrays and polycarbonate (PC) or other dielectric multilayered nanostructures can be useful in optical applications^{13–18}, such as color generation by patterned arrays of silicon nanowires^{13–15} and nanowire-based wavelength selective photodetectors¹⁶.

However, the size of unit cells of these non-plasmonic nanostructures is on the order of the wavelength of light, usually in micrometer dimensions. This means that there is still room for further improvements to reach the diffraction limit. To go beyond the natural color generation, surface plasmon resonances (SPRs) open a promising way to control colors with high efficiency and high resolution due to the development of nano-fabrication technologies. The interaction between light and plasmonic nanostructures has been shown to manipulate intensity, phase, and polarization of the scattering light^{19–27}. Thus plasmonic nanostructures are promising for use in high-resolution color displays and imaging applications due to their small dimensions and the ability to efficiently

manipulate light^{28, 29, 30}. The sub-wavelength plasmonic elements enable the structure to be ultra-thin, usually 1–2 orders of magnitude thinner than pigment-based filters, making it favourable for integration and miniaturization of display devices. Plasmonic color filters with periodic sub-wavelength hole array in a metal film can achieve high transmission efficiencies due to the phenomenon of extraordinary optical transmission (EOT)^{19, 20, 22, 31}, which is an important consideration in reducing power consumption. Moreover the energy absorbed by a multi-layer nano-grating filter can be harvested and converted to electrical energy while producing desirable colors in the visible band³², making it energy-efficient and suitable for electro-optic applications. Recently, color printing with plasmonic nanostructures has demonstrated the resolution of 100,000 dots per inch (d. p. i.), which is already at the diffraction limit³³. This high-resolution plasmonic color printing technology has significance in optical data storage, digital imaging, and in security applications. In addition, although some plasmonic nanostructures are designed to avoid incident angle dependence³⁴, it is also useful for developing active color filters with controllable output based on sensitivities to incident angle or polarization^{35, 36}. With these advantages, the plasmonic nanostructures have great potential in color filtering and imaging applications such as digital photography and digital displays.

This paper will provide an overview of the most recent development of nanostructural color filtering and imaging nanotechnologies, several kinds of representative nanostructures that perform well in color filtering and imaging or have special functionalities are presented. We will discuss the advantages and potential for practical applications as well as their limitations.

2. Color generation of plasmonic nanostructures

Surface plasmons (SPs) are collective free-electron oscillations at metal-dielectric interfaces. They exhibit enhanced near-field amplitude of electric field at the resonance wavelength. This field is highly localized and decays exponentially away from the metal/dielectric interface^{37–41}. Unlike photon absorption in pigments, which is determined by the energy level transitions of the molecules, the scattering and absorption of plasmonic nanostructures are determined by their geometry and dimensions. Leveraging on the development of nanofabrication technologies such as electron-beam lithography (EBL) and focused ion beam (FIB), the shape and size of metallic nanostructures can be well-controlled with sub-10-nm

precision^{42, 43}. With these sub-wavelength elements, the pixels of color imaging can be extremely small and the resolution can be improved up to the diffraction limit, with thickness of resonators of only tens of nanometers. In addition to the advantage of high resolution and ultrathin characteristics, plasmonic nanostructures have also the following attributes: (1) as the nanostructures are made

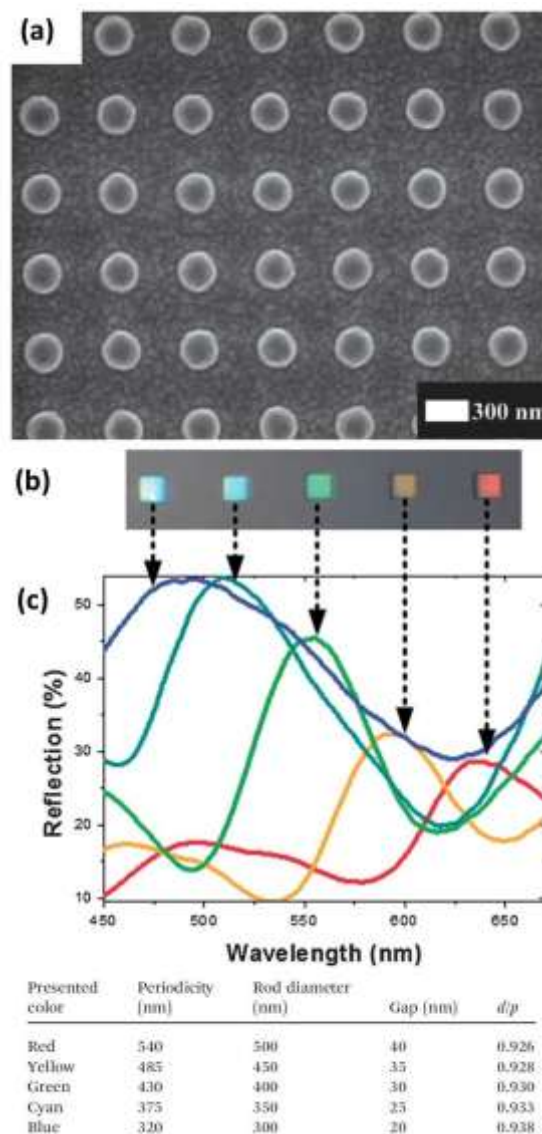


Fig 1 (a) Scanning electron microscope (SEM) image of the top view of a Ag vertical nanorods array on a quartz substrate with periodicity $p=550$ nm. (b) Optical image of the reflective colors from different Ag nanorod arrays. (c) Measured reflection spectra of the corresponding arrays as a function of wavelengths. The table below (c) shows the size parameters of nanostructures for different colors in (b) and (c). Reproduced with permission⁵⁰. Copyright 2013, RSC.

of metal, they are chemically stable and can endure long-duration ultraviolet irradiation and high temperatures compared to chemical pigments; (2) the device can realize a broad range of colors using a single element of metal, by just varying the lateral size and geometry of structures. This avoids the sequential deposition of inks, reduces process steps, and misalignment between color channels; (3) the SPRs can be tuned by factors such as environment index, incident angle and polarization, it is possible to make the optical element active^{35, 36, 44–48}, which could be useful for dense optical data archival⁴⁹, and contributes to security applications.

2.1 Structural color from localized surface plasmon resonance (LSPR)

2.1.1 Polarization-independent nanoantennas

Well-designed plasmonic nanoparticles can be viewed as optical nanoantennas that receive optical radiation from the far field to the near field at specific frequencies and vice versa. Due to the geometry- and dimension-dependence, the localized surface plasmon resonances (LSPR) of these nanoantennas can be manipulated to achieve desirable reflection and transmission spectra^{35, 46, 50, 51}, and further generate the imaging pattern with pre-designed plasmonic structures^{21, 52, 53}. A typical reflection-mode plasmonic color filter based on the silver vertical nanorod array⁵⁰, is shown in Fig. 1. To understand the mechanism, each single nanorod can be modeled by a dipole of polarizability α , and the LSPR can be estimated by the coupling dipole theory^{54, 55}. When the resonator is excited, it will radiate a scattering field in proportion to its dipole moment. The static polarizability of each resonator can be written as^{56, 57}

$$\alpha^{\text{static}} \propto V \frac{\epsilon_m - \epsilon_d}{3\epsilon_m + 3\chi(\epsilon_m - \epsilon_d)} \quad (1)$$

where ϵ_m and ϵ_d are the relative permittivities of metal and surrounding environment, respectively; χ is the geometrical factor relating to the physical shape of nanorod and V is the volume of resonator. Assuming the whole array is infinite, the effective polarizability α^* of the LSPR on single dipole resonator can be generally expressed as⁵⁷

$$\alpha^* = \frac{1}{\frac{1}{\alpha} - S} \quad (2)$$

where the array factor S for the square array with normal incidence can be written as⁵⁷

$$S = \sum_{\text{dipoles}} e^{ikr} \left[\frac{(1-ikr)(3\cos^2\theta-1)}{r^3} + \frac{k^2\sin^2\theta}{r} \right] \quad (3)$$

θ and r denote the position of dipole resonators. When the condition $S=1/\alpha$ is satisfied, the effective polarizability would be maximized, leading to a resonance of the dipole array with strong scattering. The wave scattering backward at resonance results in a reflected peak, and a transmitted dip correspondingly. Although the collective plasmonic resonances are also influenced by the Wood's anomaly and Bloch wave surface plasmon polaritons^{58–62}, which are mutually coupled and may even lead to the anti-crossing effect^{63, 64}, these expressions provide a good estimate for the color filtering mechanism of the nanoantenna array.

The dimension of the nanorods in Fig. 1a is optimized to enhance efficiency, and the reflected color is controlled by the diameter and periodicity of the nanorod array. To achieve the full color band, especially the blue color, small periodicity and high diameter/periodicity (d/p , up to 0.938) ratio of the nanostructure is required, which means the gap between two nanorods needs to be ultrasmall (about 20nm), as shown in the table in Fig. 1c. This requires high fabrication accuracy, but on the other hand, provides high resolution. The periodicity is close to the wavelength, so it is possible to form pixels that are much smaller than those of conventional chemical pigment-based methods.

2.1.2 Polarization-dependent nanoantennas

Polarization dependent color filtering and imaging provides another degree of freedom to manipulate color information^{35,36}, which is important and has potential applications in many fields. First of all, it can be applied to polarization- related measurements, such as birefringence measurements of cancerous tissues⁶⁵ and other bio-sensing applications. Secondly, it can improve data storage efficiency by having two different resonances for a single structure. The polarization dependence could at least double the information capacity by recording data in different polarization states. In addition, it can also be useful in security applications by patterned surfaces that have concealed messages that can be read out only through the right combination of polarizers.

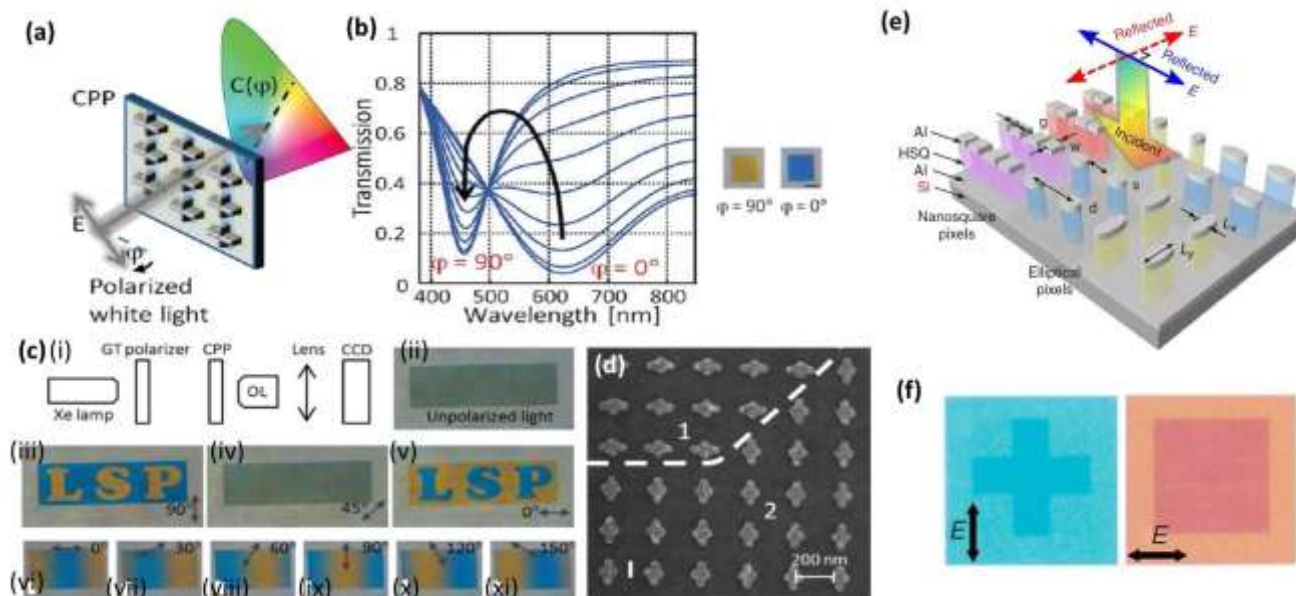


Fig 2 (a-c) Conversion of polarization state to visible color by cross nanoantennas: (a) Polarized white light is color filtered by the LSPs on the arms of the cross nanoantennas, the output color results from additive color mixing of the filtering functions of the two arms of the cross. (b) Simulated transmission spectra for linearly polarized illumination with polarization angles ranging from $\varphi = 0^\circ$, at which yellow is blocked, to $\varphi = 90^\circ$, at which blue is blocked, in steps of 10° . (c(i)–(xi)) c(i) Schematic representation of experimental setup. c(ii)–(v) Transmission images of LSP pattern sample for (ii) unpolarized incident light, (iii) 90° , (iv) 45° and (v) 0° polarized light. c(vi)–(xi) Transmission images of twisted sample for 0° – 90° polarized light in steps of 30° . (d) SEM image of part of LSP sample. (e) Schematic diagram of polarization dependent nanostructure with elliptical nano-pillars and coupled nano-square pair pillars with Al on top and at the bottom. (f) Schematic diagram of polarization dependent nanostructure with Al elliptical nano-disks and coupled nano-square pair with corresponding holes at the bottom Al layer. (f) Optical image of the same area formed from elliptical pixels with different linear polarized incident light. (a)–(d) Reproduced with permission³⁵. Copyright 2012, ACS. (e), (f) Reproduced with permission³⁶. Copyright 2014, NPG.

Due to the circular symmetry of the structures, the nanorod array responds equally to different polarized incident lights. However, the polarization dependence of the plasmonic nanostructures can also be utilized in color filtering and imaging applications. Polarization dependence of plasmonic nanostructures has been well studied in the past few years. For instance, nanostructures composed of metallic crosses with different arm lengths³⁵ exhibit strong dependence on the polarization states. As shown in Fig. 2a, b, either vertical or horizontal polarized incident light can only excite the LSPR of their corresponding arms, so that they have different transmission spectra and render different colors. At arbitrary polarization angle φ , the transmission spectra is a linear superposition of vertical and horizontal states, represented as

$$T(\varphi, \lambda) = T_V(\lambda) \sin^2 \varphi + T_H(\lambda) \cos^2 \varphi \quad (4)$$

where $T_V(\lambda)$ and $T_H(\lambda)$ are the transmittances for light polarized vertically and horizontally. An optimized design of Al cross nanostructure³⁵ can be a yellow color filter for incident polarization along their short arms while being a blue filter for incident polarization along long arms. With controlled position and rotating angle of these elements, it can achieve active polarized images. Fig. 2c(ii–v) shows a sample of acronym “LSP”. The cross nanoantennas composing the letters are identical to those in background area, but rotated 90° . Therefore, for vertical and horizontal polarized incidence, the letters show a different color to the background, but when incident light is polarized 45° , the color difference is eliminated. Fig. 2c(vi–xi) shows another example that the cross nanoantennas are patterned with a rotating angle $\theta(x) = 180^\circ x/L$, where x is the spatial coordinate and L is the extent of the sample in the x direction. As the incident polarization angle varies,

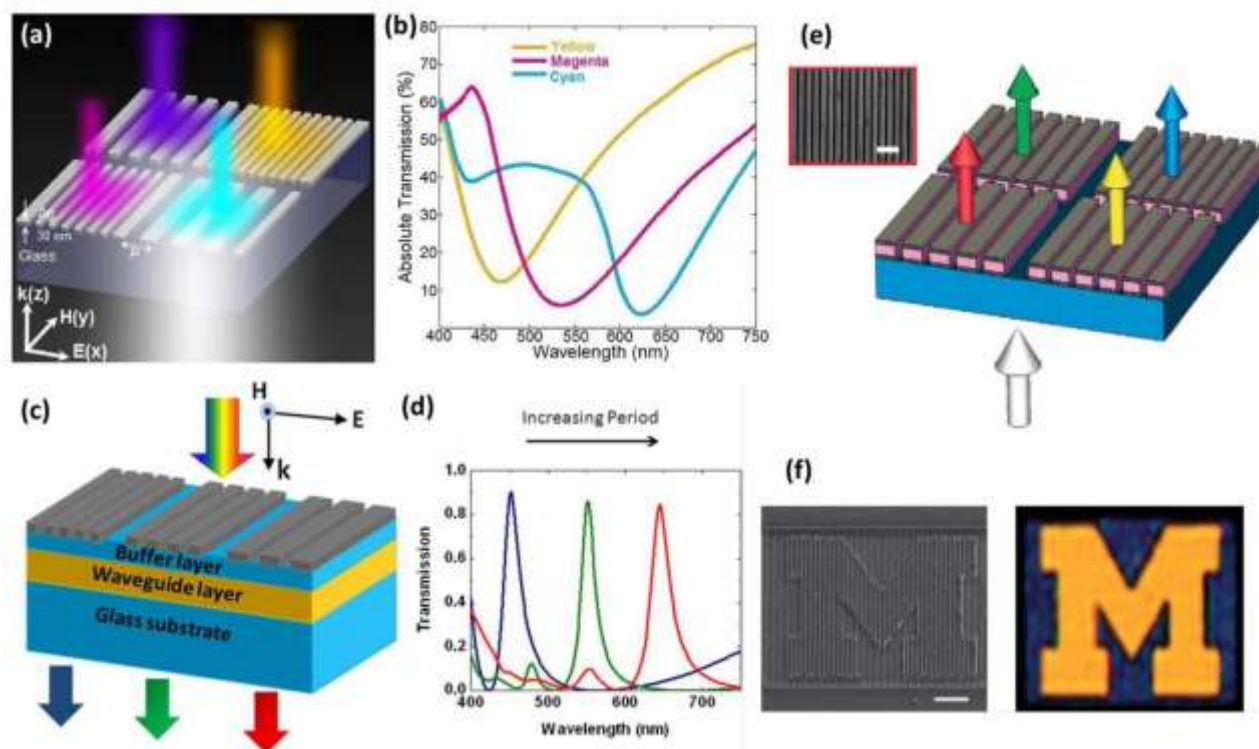


Fig 3 (a) Schematic diagram of the grating color filter of 30nm thick Ag grating with different period. (b) Measured TM transmission spectra of yellow, magenta and cyan for structure in (a). (c) Schematic of the grating color filter structure with a buffer layer. (d) Simulated transmission spectra of RGB for structure in (c). (e) Schematic diagram of MIM grating color filter. (f) SEM image and optical microscopy image of pattern “M” formed by structure in (e) illuminated by white light. (a), (b) Reproduced with permission⁶⁷. Copyright 2013, NPG. (c), (d) Reproduced with permission⁶⁹. Copyright 2011, AIP Publishing LLC. (e), (f) Reproduced with permission⁷¹. Copyright 2010, NPG.

the transmitted color image along x direction is also moving like a wave. Moreover, the practical application of this plasmonic polarization dependent color filter has been successfully demonstrated by the bright field polarized imaging of a birefringent plastic film, and on chicken breast tissue with birefringent effect of the muscle fibers.

Similar to the cross structures, pixels consisting aluminum (Al) elliptical nano-disks or coupled nano-square pair with complementary holes at the bottom Al layer³⁶, as shown in Fig. 2e, can also create different images with different polarized incident light (Fig. 2f). There nanostructure can provide abundant color in full visible range. The application of these polarization dependent disks—holes nanostructures will be further discussed in section 2.3.1.

2.1.3 Structural color from one-dimensional (1D) metallic grating

Efficiency is always an important parameter for practical applications. Metallic gratings^{32, 48, 53, 66–76}, which are also highly wavelength selective, are good candidates for highly efficient optical elements. A high transmission subtractive color filter with ultrathin 1D silver (Ag) grating with subwavelength periodicity⁶⁷ is shown in Fig. 3a. Counter-intuitively, an extraordinary low transmission (ELT) effect arises, resulting from the hybridization of LSPR and short-range surface plasmon polaritons. The ELT effect leads to a dip in the transmission spectrum. Simultaneously, since the Ag is optically thin the transmittance at off resonance wavelengths is high, which enables this nanostructure to be an efficient subtractive color filter. The efficiency of this simple 1D plasmonic grating filter would be 60-70%, which is very efficient among subtractive color filter designs.

On the other hand, high efficient additive color filters are greatly valuable as well. An Al grating⁶⁸ with a high-index dielectric waveguide layer can provide an efficiency of over 70% at

transmission peak. The color filtering is achieved by means of the guided mode resonance (GMR) effect^{77,78}. The GMR between the diffracted modes of grating and the guided modes of the planar dielectric waveguide (with Al grating as the upper cladding and quartz substrate as the lower cladding) is readily induced as long as phase matching is achieved between them. The transmission is substantially increased when incident wave constructively interferes with this coupled mode. Furthermore, as shown in Fig. 3c, a similar nanostructure but with a low-index buffer layer between the metal grating and high-index waveguide layer was reported with an improved transmittance of nearly 90%⁶⁹. The thickness of buffer layer can control the loss of the guided mode in metallic gratings, which can be explained by the theory of metal cladding dielectric waveguide⁷⁹. Therefore, this nanostructure with buffer layer can achieve narrowband resonances and high efficiency in the transmission spectra. This characteristic of high and sharp peaks is suitable for producing colors with high purity.

The resonance within the metal – insulator – metal (MIM) structures^{32, 45, 70, 71, 80–84} can be used to filter white light into individual colors as well. The most important limitation of the MIM color filters is their low transmittance, so it is valuable to introduce diffractive effects into MIM structures to improve their efficiency. In Fig. 3e, a MIM grating is constructed by Al-ZnSe-Al resonators. The bottom Al grating is used to couple the incident light into plasmon waveguide modes by diffraction, and the top Al grating reconverts the confined plasmon into propagating waves by scattering the light to far field in the forward direction, while the ZnSe layer ensures the efficient coupling of SP modes at the top and bottom Al layers. This photon – plasmon – photon conversion efficiently enhances the transmission at specific wavelength. The periodicity of this MIM grating varies from 200nm to 400nm to achieve arbitrary colors, such a small periodicity also helps attaining high resolution for color image and display (in Fig. 3f).

Overall, the most significant advantage of plasmonic grating color filter and image among the plasmonic nanostructure is their high efficiency (usually 60% to 90%). For those grating nanostructures coupled with guided modes, the bandwidth of resonance can be very narrow (with FWHM of 30 nm⁶⁹), so that the filtered color can be pure. The spatial resolution of these nanostructures is also ultrahigh, closed to the diffraction limit^{67, 71}. The period of grating can be mini-fied to half wavelength, and the length of grating can also be subwavelength, evolving to nanosquare arrays or so-called 2D

gratings. Another characteristic of 1D grating is the polarization dependence. Only transverse magnetic (TM) waves (the electric field is perpendicular to the grating direction) can be filtered, while the transverse electric (TE) waves (the electric field is parallel to the grating direction) will be mostly reflected or transmitted. Therefore they can actively work for many polarization-related applications as discussed in section 2.1.2.

2.2 Structural color from propagating surface plasmon

As discussed in section 2.1, the LSPR in metallic nanoantennas produces peaks in reflection spectrum and dips in transmission spectrum. According to the Babinet's principle⁸⁵, the complements of these nanoantennas, which are the hole arrays in metal films, would result in dips in the reflection spectra and peaks in the transmission spectra. While nanoantenna arrays can work as subtractive color filters in transmission mode, nanohole arrays on metallic film can work as additive filters, which are needed in many imaging and display applications.

Considering a single hole in a metallic film, the transmission efficiency should be proportional to $(r/\lambda)^4$, where λ is the incident wavelength and r is the radius of the hole^{86, 87}. It means the transmission of subwavelength hole would be extremely low. However, the periodic metallic structures can provide the momentum for converting incident light into SPs, so that the hole array on the metal film can give rise to the EOT effect^{19, 20, 22}. In the past few years, the hole arrays had been theoretically and experimentally^{88–107} studied in many aspects, such as the selective extraordinary transmission for color filtering. The wavelength of transmission peak λ_{\max} depends on the periodicity and the constituent of the hole array. At normal incidence, for the square array

$$\lambda_{\max} = \frac{a}{\sqrt{i^2 + j^2}} \sqrt{\frac{\epsilon_m \epsilon_d}{\epsilon_m + \epsilon_d}} \quad (5)$$

and for the hexagonal array

$$\lambda_{\max} = \frac{a}{\sqrt{\frac{4}{3}(i^2 + ij + j^2)}} \sqrt{\frac{\epsilon_m \epsilon_d}{\epsilon_m + \epsilon_d}} \quad (6)$$

where a is the periodicity of array, ϵ_m and ϵ_d are the relative permittivities of metal and dielectric material, and i and j are the

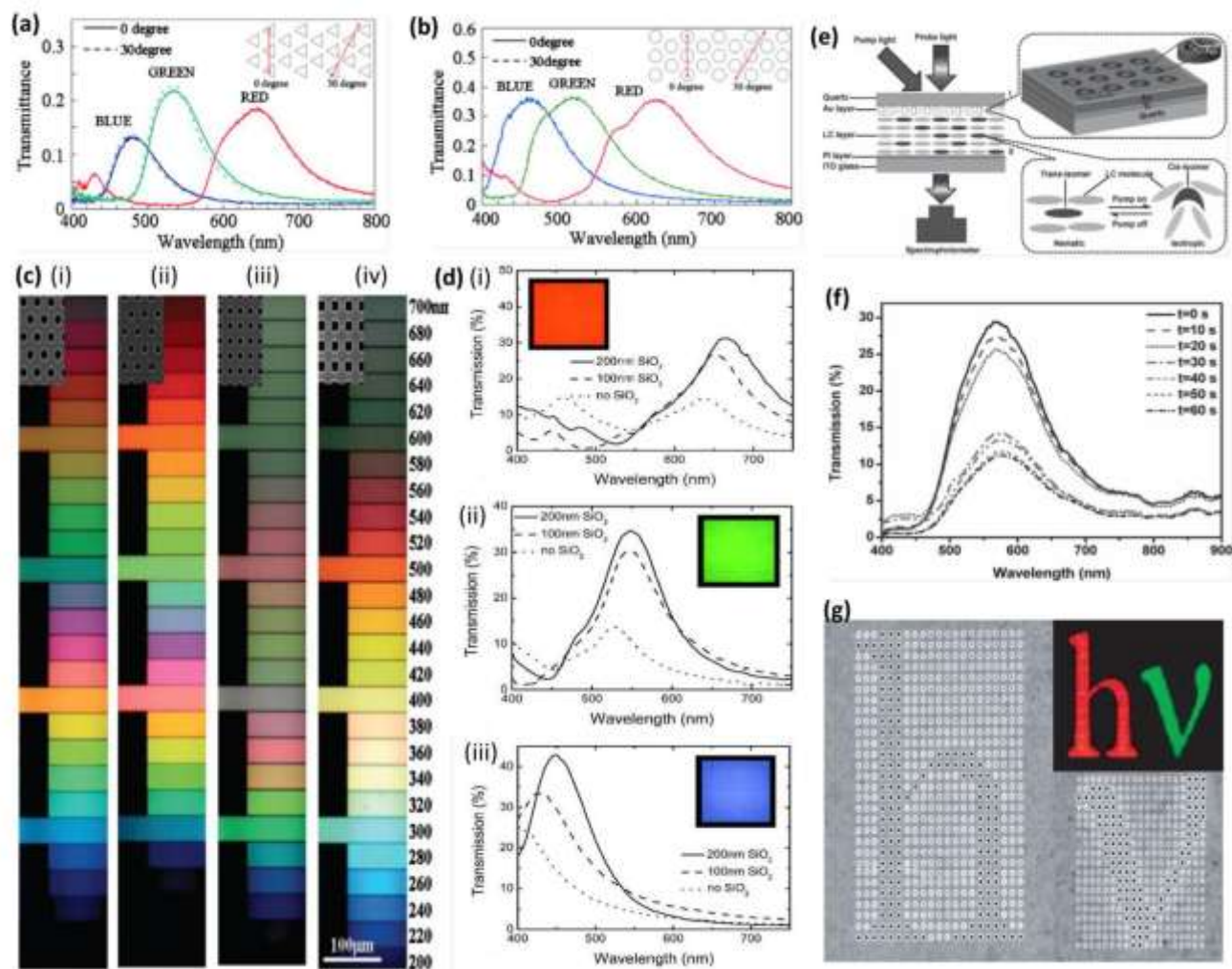


Fig 4 (a-b) Polarization dependence of the transmission spectra of RGB color filters with (a) triangular holes and (b) circular holes in hexagonal array. (c(i)–(iv)) Optical microscope images of Al color filters with (i) circular holes in hexagonal array, (ii) triangular holes, (iii) circular holes in square array, and (iv) square holes. (d(i)–(iii)) Measured transmission spectra of RGB color filters of circular hole array, with no cap layer, 100 nm and 200 nm SiO₂ cap layer. (e) Schematic of the sample structure and experimental setup for color filter with LC layer. The zoom-in part I shows the fabricated square pattern of Au AAAs, and the zoom-in part II shows the working mechanism of the optical driving process in LCs. (f) The evolution of the transmission spectra as a function of time under the UV pump for the color filter with an aperture size of 120 nm. (g) Holes in a dimple array generating the letters “hv” in transmission, with period of 550nm (red color) and 450nm (green color). (a)–(c) Reproduced with permission¹¹¹. Copyright 2011, AIP Publishing LLC. (d) Reproduced with permission¹⁰⁸. Copyright 2010, OSA. (e), (f) Reproduced with permission⁴⁷. Copyright 2012, John Wiley and Sons. (g) Reproduced with permission⁸⁶. Copyright 2007, NPG.

scattering orders of the array^{86, 108, 109}. Considering the interference of the scattering losses of the holes and the Fano-type interaction^{62, 110}, λ_{\max} would be slightly blue shifted. Based on the interaction of these modes, the hole arrays can be designed for transmitted color filters.

In particular, for the lowest order mode ($i = \pm 1, j = 0$), the SPR peak wavelength of hexagonal array is smaller than that of square array

with the same period and material. Moreover, the wavelength interval of transmission peak between the first two modes of hexagonal array is also larger, which makes hexagonal array more

favorable to reduce the color cross-talk and improve the purity of color. To a lesser extent, the shape of holes also affects the color, as shown in Fig. 4a, b. The triangular hole arrays give narrower resonance peaks than the circular hole arrays, but with lower

efficiency. After comparing, it is also found that lattice construction has larger influence on than hole shapes. Interestingly, the hexagonal array performs much better in building a full color map.

In experiments, the metallic film with hole array is usually fabricated on a glass substrate, which leads to an asymmetric dielectric environment. Therefore, two SP modes on both sides are resonant at different wavelengths, which would reduce the color purity due to peaks overlapping. Owing to such asymmetry, momentum mismatch also results in an inefficient coupling between two sides and then a moderate transmittance. In order to deal with this, an index-matching layer is used to coat the air side¹⁰⁸. As an example shown in Fig. 4d, the transmittance was efficiently improved in the presence of SiO₂ layer in comparing with the case in the absence of SiO₂.

As indicated by eqn (1) and (2), the transmission peak could be readily modulated by varying the refractive index of environment. Recently, an active plasmonic color filter was introduced by overlaying photoresponsive liquid crystals (LCs) onto gold (Au) annular aperture arrays (AAAs)⁴⁷, as shown in Fig. 4e. The photochromic LC molecules would change their form upon UV irradiation, and further generate a photoinduced refractive index modulation. The transmittance could be greatly reduced as shown in Fig. 4f. Through further improving the tunability of plasmonic color filters with active optical control, an active display might be possible if the RGB compositions could be separately controlled.

The resolution of the metallic hole arrays is much higher than that of chemical pigments, but it could not reach the diffraction limit yet. For example, a color filter with different structures¹¹¹ is shown in Fig. 4c, while an image of “hv” is displayed with square hole array⁸⁶ in Fig. 4g. The periodicities are all larger than half of the corresponding wavelength, sometimes almost comparable to the wavelength.

Overall, the resolution of these nanohole arrays can already satisfy the requirement of most practical applications, with just last step to the theory limitation. And they can also provide a variety of colors with promising visual effects, as shown in Fig. 4c. However, the transmission efficiency of nanohole arrays is relatively low compared to those color filter utilizing grating nanostructures.

2.3 Structural color from plasmonic mode coupling

2.3.1 Structural color from nanodisks-nanoholes

In previous sections we have introduced some representative works on color filtering and imaging, based on either localized or propagating SPs. However, in terms of resolution color imaging, there is still plenty room for improvement to approaching the diffraction limit since the plasmonic nanostructures discussed previously (nanoantenna arrays, hole arrays, 1D gratings) have pixel sizes comparable to the wavelength. Here a coupled plasmonic nanostructure which can produce pixels smaller than half-wavelength is introduced. The representative nanostructure contains a metallic nanodisk suspended on top of a dielectric pillar and a complementary metallic hole as a back reflector^{33, 36, 112–115}. The top disks provide LSPRs and the back reflector provides propagating SPs, and the height of the dielectric pillars determines the coupling between them. It has been used for ultrahigh and uniform surface-enhanced Raman scattering¹¹⁴, and demonstrating extraordinary light transmission effect with transparent substrate¹¹³. A high resolution nano-printing technology at diffraction limit was reported based on this nanostructure³³, by depositing a thin layer of Au-Ag on hydrogen silsesquioxane (HSQ) pillars on a silicon substrate. By manipulating the separation between pillars and the sizes of the metal top disks, the coupling between the resonances of disks and the back reflector can be tuned to affect the reflected color.

As shown in Fig. 5a, b, a color map is achieved by nanostructures with different gap size (g) and disk size (D), providing also some really dark colors. It should be noted that the periodicity (D+g) varies from only 80 to 260 nm. In Fig. 5c, an image of *Lena* is produced by nanostructures with the same periodicity (125 nm) and different disk sizes. Such a small size of nanostructure ensures a resolution at the optical diffraction limit. To enrich the color gamut and increase the practicality of this nano-printing technology, the constitute materials Au and Ag are replaced by Al, which is a more preferable metal for plasmonic color printing because of its neutral tint, durability, high reflectance in the visible regime, and low cost. With varied gap and disk size, individual pixels are constructed by mixing disks of different sizes¹¹². To complement the limited color palette produced by just modifying gap and disk sizes, dual-size-disk pixels (2×2 disks array mixed with different sizes) are constructed, which greatly increased the range of colors and provided an approach for plasmonic color mixing (Fig. 5d,e). The comparison of “basic” color palette by varying just the Au—Ag disk sizes and the “color-mixing” palette is shown in the micrographs in Fig. 5f, g. Color mixing provides an accurate reproduction of Monet’s *Impression, Sunrise* painting that was poorly reproduced by the

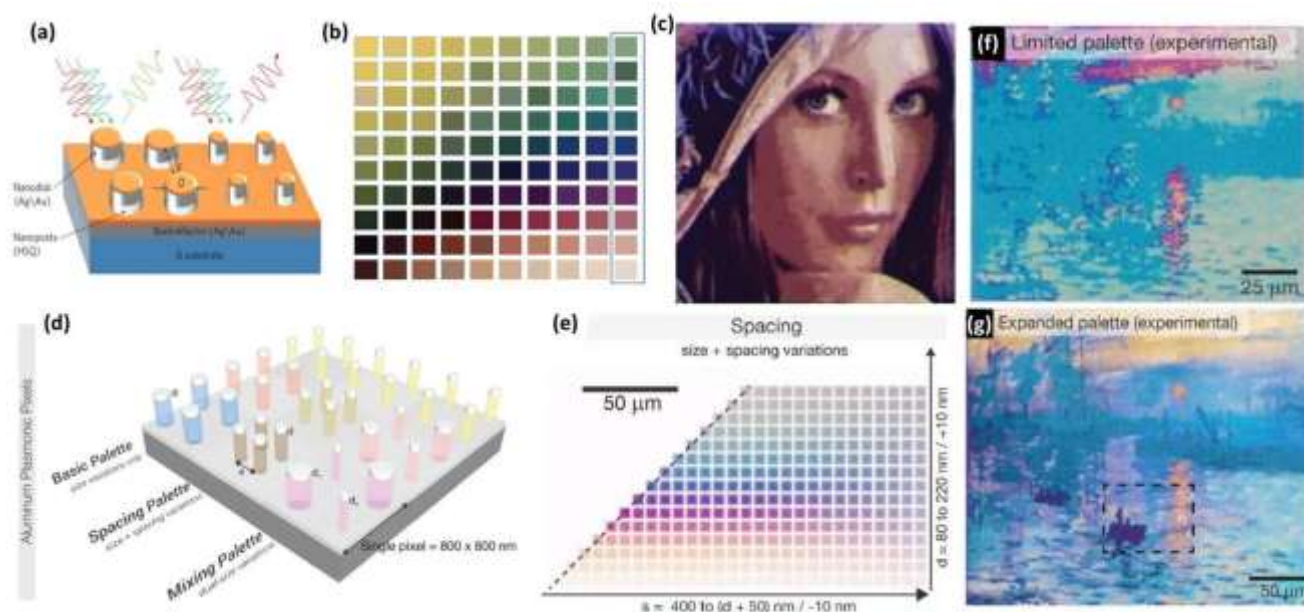


Fig 5 (a) Plasmonic color pixels composed of isolated Au/Ag nanodisks structures set against a back reflector. (b) Full color palette with disk size $D=50$ — 140nm , gap size $g=30$ — 120nm produced by pixels in (a). (c) Optical micrographs of the Lena image produced by pixels in (a). (d) Plasmonic color pixels composed of Al nanodisks with back reflector of varying disk size palette, varying disk size and spacing palette and mix-disks palette. (e) Full color palette for pixels in (d). (f-g) Reproduction of Monet's *Impression, Sunrise* using (f) basic colors and (g) the expanded colors in (e). (a)—(c) Reproduced with permission³³. Copyright 2012, NPG. (d)—(g) Reproduced with permission¹¹². Copyright 2014, ACS.

primary plasmonic color palette. Further research based on the disk-and-back-reflector-coupled nanostructures realizes 3D plasmonic stereoscopic prints utilizing their polarization dependence³⁶. Using biaxial color pixels composed of elliptical nanodisk-hole structures (shown in Fig. 2e) can independently control the reflected spectra of orthogonal polarized incident lights, so that two different color images can be encoded into the same area. Therefore, the stereoscopic effects can be achieved by fine modulation of the differences between two images with different polarization.

2.3.2 Structural color from other plasmonic nanostructures

Plasmonic nanostructures for color filtering and imaging can also be achieved based on other characteristic and mechanisms^{34, 115, 116}. For example, a MIM nanostructure containing Au nanodisk array hovering on a Au film with a thin dielectric layer in between, is capable of supporting gap-surface plasmons (GSPs)^{115, 117, 118}. By

tuning the size of disks and the thickness of dielectric layer, the reflected color can be tuned flexibly (Fig. 6a, b). This nanostructure with GSPs has its own advantages compared to many other plasmonic color nanostructures. Firstly, the reflection spectra are insensitive to the incident angle which is valuable in practical applications. Secondly, while the colors of most plasmonic nanostructures are sensitive to the environmental index, this nanostructure can endure a cover of transparent dielectric overlay without shifting much in color. In Fig. 6c, an optical microscopy image is shown to compare the colors of uncovered (left) and dielectric covered (right) parts of the color printing, and overall color image remains except for a slight contrast variation. Therefore this plasmonic color device can be protected by coating a transparent layer without destroying the color, which enables its ambient usability.

Another incident angle independent case is based on Fabry - Perot (FP) cavity modes³⁴. The structure is shown in Fig. 6d, and the dimensions and periodicity of the structure have been designed to

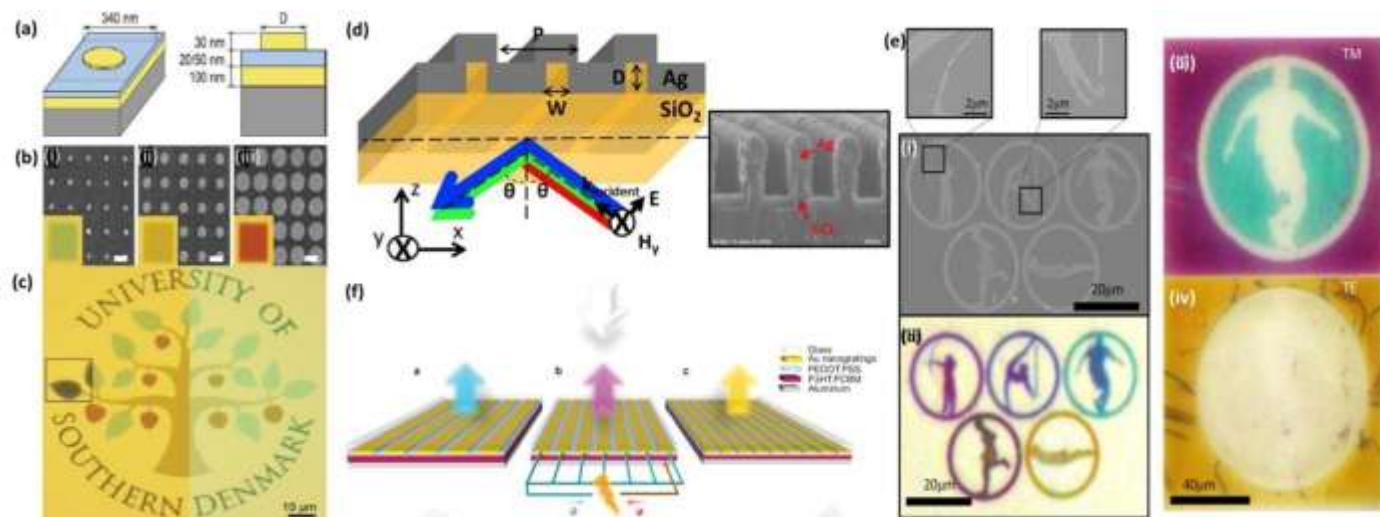


Fig 6 (a) Schematic views of a unit cell of a MIM structure with Au (yellow) nanodisk on SiO₂ (blue) layer and Au layer. (b)(i)–(iii) SEM images of nanodisks with average sizes of (i) 80, (ii) 120, and (iii) 270 nm. (c) Optical microscopy images with pixels in (a) comparing an uncovered color print (left) and the same print (right) after covering the sample with 100 nm of PMMA. (d) Schematic of light funnelling nanostructure and corresponding SEM image. (e)(i)–(iv) The (i) SEM images and (ii) optical image under white light illumination of fabricated Olympic rings. (iii) TM and (iv) TE polarized light illuminating image of one of the Olympic rings. (f) Schematic of dual-function devices for both color filtering and electrical powers generating. (a)–(c) Reproduced with permission¹¹⁵. Copyright 2014, ACS. (d), (e) Reproduced with permission³⁴. Copyright 2013, NPG. (f) Reproduced with permission³². Copyright 2011, ACS.

avoid plasmonic modes excitation relying on grating coupling, which are highly dependent on incident angles. Instead, the nanostructures concentrate light into the silica nano-grooves based on light funnelling of FP cavity modes. At the designed wavelength, the absorptance can reach over 90% within ± 90 degree angle range for specific structure dimensions, so that it performs well as an angle-independent subtractive reflective color filter. The periodicity of this plasmonic nanostructure is also beyond the diffraction limit of light, thus it can produce polarization-dependent high resolution image, as shown in Fig. 6e.

In addition, the plasmonic color filter can also be integrated with organic solar cells³². As shown in Fig. 6f, the MIM nanostructure contains Au nano-grating on top and Al film at the bottom, which serve not only as a plasmonic color filter, but also as electrodes for the organic photovoltaic (OPV) cells. By manipulating the periodicity of grating and the thickness of photoactive layer, incident light at specific wavelength can be directly absorbed and then transferred into photocurrents by the OPV structure instead of wasting as heat, which indicates the great potential of plasmonic nanostructures in electrooptic applications.

3. Summary and outlook

We have reviewed the recent development of plasmonic colors generated by nanostructures. Compared to the conventional pigments and the non-plasmonic structural colors, plasmonic color shows more advantages including ultrasmall dimensions, impressive optical response, wide color tunability and compatibility for device integration. Nano-scaled size of plasmonic structures enables image printing at high resolutions, even beyond the optical diffraction limit. Most structures simply contain one or several ultrathin layers of metallic/dielectric materials, so that their thickness is only tens or hundreds of nanometers. This thin geometry makes them easy for integration with miniaturized devices. The well-controlled plasmonic resonance also provides wide color range and accurately distinguished color. Moreover, diversity of plasmonic nanostructures contributes in achieving specific targets, such as high efficiency in transmission or reflection, narrower band-width for purer color, reduced incident angle dependence, tunable polarization applications, and electro-optic modulations.

Although plasmonic nanostructures have so many advantages and great potential in next generation color relevant applications, the first commercial applications would require a drastic reduction in patterning costs. Fabrication methods such as EBL and FIB are necessary to create master templates from which high-throughput replication processes such as nanoimprint can be used to create large volume of copies. The commonly used plasmonic materials, Au and Ag, are also expensive for mass production, leading to the recent trend to use Al, which is also CMOS compatible. In addition to cost reduction, the performance of plasmonic devices needs to be comparable or better than existing technologies. For instance, in the application of plasmonic color filters for digital imaging products, the limiting factor is still the insufficient transmittance when compared to pigment-based filters. Hence, while many novel phenomena have been reported in literature, a strong need now is to significantly improve the optical performance of plasmonic color structures.

In summary, plasmonic nanostructures show great potential in development of color filtering, high-resolution display and imaging, optical data storage and security. With improved low-cost fabrication technology, they are slated to offer improved performance and lower cost in applications ranging from digital displays, imaging sensors, molecular sensing, optical security devices, and optical data archival.

Acknowledgements

The authors acknowledges the support from the National University of Singapore (Grant R-263-000-A45-112).

Notes and references

^a Department of Electrical and Computer Engineering, National University of Singapore, Singapore 117583, Singapore.

^b Institute of Materials Research and Engineering, Agency for Science, Technology and Research, 3 Research Link, Singapore 117602, Singapore

^c Singapore University of Technology and Design, Engineering Product Development, Singapore 138682, Singapore.

Reference

1. Y. Huo, C. C. Fesenmaier and P. B. Catrysse, *Opt. Express*, 2010, **18**, 5861.
2. H. Koo, M. Chen and P. Pan, *Thin Solid Films*, 2006, **515**, 896.
3. M. C. Gather, A. K'ohnen, A. Falcou, H. Becker and K. Meerholz, *Adv. Funct. Mater.*, 2007, **17**, 191.

4. E. Abbe, *Proc. Bristol Nat. Soc.*, 1874, **1**, 200.
5. P. Vukusic, J. R. Sambles, *Nature* 2003, **424**, 852.
6. M. Sinivasarao, *Chem. Rev.*, 1999, **99**, 1935.
7. J. Huang, X. Wang and Z. L. Wang, *Nano Lett.* 2006, **6**, 2325.
8. T. S. Kustandi, H. Y. Low, J. H. Teng, I. Rodriguez and R. Yin, *Small*, 2009, **5**, 574.
9. P. Vukusic, J. R. Sambles, C. R. Lawrence and R. J. Wootton, *Proc. R. Soc. Lond. B* , 1999, **266**, 1402.
10. S. Kinoshita, S. Yoshioka and K. Kawagoe, *Proc. R. Soc. Lond. B.* 2002, **269**, 1417.
11. H. Ghiradella, *Appl. Opt.*, 1991, **30**, 3492.
12. C. R. Lawrence, P. Vukusic and J. R. Sambles, *Appl. Opt.*, 2002, **41**, 437.
13. L. Cao , P. Fan , E. S. Barnard , A. M. Brown and M. L. Brongersma, *Nano Lett.*, 2010, **10**, 2649.
14. M. Khorasaninejad, N. Abedzadeh, J. Walia, S. Patchett, and S. S. Saini, *Nano Lett.*, 2012, **12**, 4228
15. K. Seo, M. Wober, P. Steinvurzel, E. Schonbrun, Y. Dan, T. Ellenbogen, and K. B. Crozier, *Nano Lett.* 2011, **11**, 1851
16. H. Park, Y. Dan, K. Seo, Y. J. Yu, P. K. Duane, M. Wober and K. B. Crozier, *Nano Lett.*, 2014, **14**, 1804.
17. V. R. Shrestha, S.-S. Lee, E.-S. Kim and D.-Y. Choi, *Sci. Rep.*, 2014, **4**, 4921.
18. Z. Wu, D. Lee, M. F. Rubner and R. E. Cohen, *Small*, 2007, **3**, 1445.
19. T. Ebbesen, H. Lezec, H. Ghaemi, T. Thio and P. Wolff, *Nature*, 1998, **86**, 1114.
20. S. Enoch, E. Popov, M. Nevier and R. Reinisch, *J. Opt. A: Pure Appl. Opt.*, 2002, **4**, 83.
21. W. T. Chen, K.-Y. Yang, C.-M. Wang, Y.-W. Huang, G. Sun, I.-D. Chiang, C. Y. Liao, W.-L. Hsu, H. T. Lin, S. Sun, L. Zhou, A. Q. Liu and D. P. Tsai, *Nano Lett.*, 2014, **14**, 225.
22. W. Fan, S. Zhang, B. Minhas, K. J. Malloy and S. R. J. Brueck, *Phys. Rev. Lett.*, 2005, **94**, 033902 .
23. G. Li, M. K., S. Chen, S. Zhang, E. Y.-B. Pun, K. W. Cheah and J. Li, *Nano Lett.*, 2013, **13**, 4148.
24. L. Meng, D. Zhao, Q. Li and M. Qiu, *Opt. Express*, 2013, **21**, A111.
25. N. Yu, F. Aieta, P. Genevet, M. A. Kats, Z. Gaburro and F. Capasso, *Nano Lett.*, 2012, **12**, 6328.
26. N. Yu, P. Genevet, M. A. Kats, F. Aieta, J.-P. Tetienne, F. Capasso, Z. Gaburro, *Science*, 2011, **334**, 333.
27. X. Chen, L. Huang, H. Mu'hlenbernd, G. Li, B. Bai, Q. Tan, G. Jin, C.-W. Qiu, S. Zhang and T. Zentgraf, *Nat. Commun.*, 2012, **3**, 1198.
28. S. J. Tan, X. M. Goh, Y. M. Wang, J. K. W. Yang and J. Teng, *J. Mol. Eng. Mater.*, 2014, **02**, 1440011.
29. T. Xu, H. Shi, Y.-K. Wu, A. F. Kaplan, J. G. Ok and L. J. Guo, *Small*, 2011, **7**, 3128.

30. Y. Yu, L. Wen, S. Song and Qin Chen, *Journal of Nanomaterials*, 2014, **2014**, 212637.
31. H. Liu and P. Lalanne, *Nature*, 2008, **452**, 728.
32. H. J. Park, T. Xu, J. Y. Lee, A. Ledbetter, and L. J. Guo, *ACS Nano*, 2011, **5**, 7055.
33. K. Kumar, H. Duan, R. S. Hegde, S. C. W. Koh, J. N. Wei and J. K. W. Yang, *Nat. Nanotechnol.*, 2012, **7**, 557.
34. Y.-K. R. Wu, A. E. Hollowell, C. Zhang and L. J. Guo, *Sci. Rep.*, 2013, **3**, 1194.
35. T. Ellenbogen, K. Seo and K. B. Crozier, *Nano Lett.*, 2012, **12**, 1026.
36. X. M. Goh, Y. Zheng, S. J. Tan, L. Zhang, K. Kumar, C. W. Qiu and J. K.W. Yang, *Nat. Commun.* 2014, **5**, 5361
37. A. V. Zayatsa, I. I. Smolyaninovb, A. A. Maradudinc, *Physics Reports*, 2005, **408**, 131–314
38. E. Ozbay, *Science*, 2006, **311**, 189.
39. E. Laux, C. Genet, T. Skauli and T. W. Ebbesen, *Nat. Photonics*, 2008, **2**, 161.
40. W. L. Barnes, A. Dereux and T. W. Ebbesen, *Nature*, 2003, **424**, 824.
41. W. L Barnes, *J. Opt. A: Pure Appl. Opt.*, 2006, **8**, 87
42. H. Duan, H. Hu, K. Kumar, Z. Shen, J. K.W. Yang, *ACS Nano*, 2011, **5**, 7593.
43. H. Duan, H. Hu, H. K. Hui, Z. Shen, J. K W Yang, *Nanotechnology*, 2013, **24**, 185301 .
44. Y. J. Liu, G. Y. Si, E. S. P. Leong, B. Wang, A. J. Danner, X. C. Yuan, J. H. Teng, *Appl. Phys. A*, 2012, **107**, 49.
45. K. Diest, J. Dionne, M. Spain and H. Atwater, *Nano Lett.*, 2009, **9**, 2579.
46. C. Saeidi, D. van der Weide, *Opt. Express.*, 2014, **22**, 12499.
47. Y. J. Liu, G. Y. Si, E. S. P. Leong, N. Xiang, A. J. Danner and J. H. Teng, *Adv. Mater.*, 2012, **24**, 131.
48. M. J. Uddin and R. Magnusson, *IEEE Photonics Technology Letters*, 2012, **24**, 1552.
49. P. Zijlstra, J. W. M. Chon and Min Gu, *Nature*, 2009, **459**, 410
50. G. Si, Y. Zhao, J. Lv, M. Lu, F. Wang, H. Liu, N. Xiang, T. J. Huang, A. J. Danner, J. Teng and Y. J. Liu, *Nanoscale*, 2013, **5**, 6243.
51. J. Do, M. Fedoruk, F. Jäckel and J. Feldmann, *Nano Lett.*, 2013, **13**, 4164.
52. L.L. Huang, X. Chen, H. Muhlenbernd, H. Zhang, S. Chen, B. Bai, Q. Tan, G. Jin, K.-W. Cheah, C.-W. Qiu, J. Li, T. Zentgraf, and S. Zhang, *Nat. Commun.*, 2013, **4**, 2808.
53. J.J. Cowan, *Opt. Commun.*, 1972, **5**, 2.
54. S. Zou and G. C. Schatz, *Nanotechnology*, 2006, **17**, 2813.
55. V. A. Markel and A. K. Sarychev, *Phys. Rev. B: Condens. Matter Mater. Phys.*, 2007, **75**, 085426.
56. C. Bohren and D. Huffman, *Absorption and Scattering of Light by Small Particles*, 1983, John Wiley & Sons, New York.
57. B. Auguie and W. L. Barnes, *Phys. Rev. Lett.*, 2008, **101**, 143902.
58. F. J. García de Abajo, *Rev. Mod. Phys.*, 2007, **79**, 1267.
59. R. W. Wood, *Philos. Mag.*, 1902, **4**, 396.
60. V. G. Kravets, F. Schedin, and A. N. Grigorenko, *Phys. Rev. Lett.*, 2008, **101**, 087403.
61. K. Lee and P. Wei, *Small*, 2010, **6**, 1900.
62. M. Sarrazin, J.-P. Vigneron and J.-M. Vigoureux, *Phys. Rev. B*, 2003, **67**, 085415.
63. L. Shao, K.C. Woo, H. Chen, Z. Jin, J. Wang and H.-Q. Lin, *ACS Nano*, 2010, **4**, 3053.
64. C. J. Tang, P. Zhan, Z. S. Cao, J. Pan, Z. Chen and Z. L. Wang, *Phys. Rev. B*, 2011, **83**, 041402.
65. J. Strasswimmer, M. C. Pierce, B. H. Park, V. Neel, J. F. de Boer, *J. Biomed. Opt.*, 2004, **9**, 292.
66. Q. Chen, C. Martin and D. R. S. Cumming, *Plasmonics*, 2012, **7**, 755.
67. B. Zeng, Y. Gao and F. J. Bartoli, *Sci. Rep.*, 2013, **3**, 2840.
68. Y.-T. Yoon, C.-H. Park, and S.-S. Lee, *Applied Physics Express*, 2012, **5**, 022501.
69. A. F. Kaplan, T. Xu, and L. J. Guo, *Appl. Phys. Lett.*, 2011, **99**, 143111.
70. Y. Chen and W. Liu, *Opt. Lett.*, 2012, **37**, 1.
71. T. Xu, Y.-K. Wu, X. Luo and L. J. Guo, *Nat. Commun.*, 2010, **1**, 59.
72. D. C. Skigin and R. A. Depine, *Phys. Rev. Lett.*, 2005, **95**, 217402.
73. Z. Sun, Y. S. Jung and H. K. Kim, *Appl. Phys. Lett.*, 2003, **83**, 3021.
74. J. A. Porto, F. J. García-Vidal and J. B. Pendry, *Phys. Rev. Lett.*, 1999, **83**, 2845.
75. A. Barbara, P. Quémerais, E. Bustarret and T. Lopez-Rios, *Phys. Rev. B*, 2002, **66**, 161403.
76. N. Nguyen-Huu, Y.-L. Lo, and Y.-B. Chen, *Opt. Commun.*, 2011, **284**, 2473.
77. N. Ganesh, A. Xiang, N. B. Beltran, D. W. Dobbs and B. T. Cunningham, *Appl. Phys. Lett.*, 2007, **90**, 081103.
78. D. W. Dobbs, I. Gershkovich and B. T. Cunningham, *Appl. Phys. Lett.*, 2006, **89**, 123113.
79. H. Nishihara, M. Haruna and T. Suhara, *Optical Integrated Circuits*, 1989, McGraw-Hill, New York
80. P. Chen, R. Liang, Q. Huang, Z. Yu, and X. Xu, *Opt. Express*, 2011, **19**, 7633.
81. L. Zhang, J. Hao, H. Ye, S. P. Yeo, M. Qiu, S. Zouhdid and C.-W. Qiu, *Nanoscale*, 2013, **5**, 3373.
82. Y.-T. Yoon and S.-S. Lee, *Opt. Express*, 2010, **18**, 5344.
83. L. Frey, P. Parrein, J. Raby, C. Pellé, D. Héroult, M. Marty and J. Michailos, *Opt. Express*, 2011, **19**, 13073.
84. A. F. Kaplan, T. Xu, Y. Wu, and L. J. Guo, *J. Vac. Sci. Technol. B*, 2010, **28**, C6O60.

85. M. Born and E. Wolf, *Principles of Optics*, 1999, Cambridge University Press, Cambridge.
86. C. Genet and T. W. Ebbesen, *Nature*, 2007, **445**, 39.
87. H. A. Bethe, *Phys. Rev.* 1944, **66**, 163
88. L. Lin and A. Roberts, *Appl. Phys. Lett.*, 2010, **97**, 061109.
89. K. Walls, Q. Chen, S. Collins, D. R. S. Cumming and T. D. Drysdale, *IEEE Photonics Technology Letters*, 2012, **24**, 602.
90. H.-S. Lee, Y.-T. Yoon, S.-S. Lee, S.-H. Kim and K.-D. Lee, *Opt. Express*, 2007, **15**, 15457.
91. G. Si, Y. Zhao, H. Liu, S. Teo, M. Zhang, T. J. Huang, A. J. Danner and J. Teng, *Appl. Phys. Lett.*, 2011, **99**, 033105.
92. A. Degiron, H. J. Lezec, W. L. Barnes, and T. W. Ebbesen, *Appl. Phys. Lett.* 2002, **81**, 4327.
93. Y. M. Strelniker and D. J. Bergman, *Phys. Rev. B*, 1999, **59**, R12763.
94. E. Popov, M. Neviere, S. Enoch, and R. Reinisch, *Phys. Rev. B*, 2000, **62**, 16100 .
95. F. I. Baida, and D. Van Labeke, *Opt. Commun.*, 2002, **209**, 17.
96. P. Lalanne, , J. C. Rodier, and J. P. Hugonin, *J. Opt. Pure Appl. Opt.*, 2005, **7**, 422.
97. V. Lomakin, and E. Michielssen, *Phys. Rev. B*, 2005, **71**, 235117.
98. F. J. Garcia de Abajo, J. J. Saenz, I. Campillo and J. S. Dolado, *Opt. Express*, 2006, **14**, 7.
99. S.-H. Chang, S. K. Gray and G. C. Schatz, *Opt. Express*, 2005, **13**, 3150.
100. W. L. Barnes, W. A. Murray, J. Dintinger, E. Devaux and T. W. Ebbesen, *Phys. Rev. Lett.*, 2004, **92**, 107401.
101. J. Prikulis, P. Hanarp, L. Olofsson, D. Sutherland and M. Kall, *Nano Lett.*, 2004, **4**, 1003.
102. K. J. Klein Koerkamp, S. Enoch, F. B. Segerink, N. F. van Hulst and L. Kuipers, *Phys. Rev. Lett.*, 2004, **92**, 183901.
103. A. Degiron and T. W. Ebbesen, *J. Opt. Pure Appl. Opt.*, 2005, **7**, 90.
104. Y.-H. Ye and J.-Y. Zhang, *Opt. Lett.*, 2005, **30**, 1521.
105. Q.-J. Wang, J.-Q. Li, C.-P. Huang, C. Zhang and Y.-Y. Zhu, *Appl. Phys. Lett.*, 2005, **87**, 091105.
106. D. Egorov, B. S. Dennis, G. Blumberg and M. I. Haftel, *Phys. Rev. B*, 2004, **70**, 033404.
107. E. Altewischer, M. P. van Exter and J. P. Woerdman, *J. Opt. Soc. Am. B*, 2003, **20**, 1927.
108. Q. Chen and D. R. S. Cumming, *Opt. Express*, 2010, **18**, 14056.
109. H. F. Ghaemi, T. Thio, D. E. Grupp, T. W. Ebbesen and H. J. Lezec, *Phys. Rev. B*, 1998, **58**, 6779.
110. C. Genet, M.P. van Exter and J.P. Woerdman, *Opt. Commun.*, 2003, **225**, 331.
111. D. Inoue, A. Miura, T. Nomura, H. Fujikawa, K. Sato, N. Ikeda, D. Tsuya, Y. Sugimoto and Y. Koide, *Appl. Phys. Lett.*, 2011, **98**, 093113.
112. S. J. Tan, L. Zhang, D. Zhu, X. M. Goh, Y. M. Wang, K. Kumar, C.-W. Qiu and J. K. W. Yang, *Nano Lett.*, 2014, **14**, 4023.
113. W.-D. Li, J. Hu and S. Y. Chou, *Opt. Express*, 2011, **19**, 21098.
114. W.-Di Li, F. Ding, J. Hu and S. Y. Chou, *Opt. Express*, 2011, **19**, 3925.
115. A. S. Roberts, A. Pors, O. Albrektsen, and S. I. Bozhevolnyi, *Nano Lett.*, 2014, **14**, 783.
116. J. Zhang, J.-Y. Ou, N. Papasimakis, Y.Chen, K. F. MacDonald and N. I. Zheludev, *Opt. Express*, 2011, **19**, 23279.
117. N. Liu, M. Mesch, T. Weiss, M. Hentschel and H. Giessen, *Nano Lett.*, 2010, **10**, 2342.
118. Y. Chu and K. B. Crozier, *Opt. Lett.*, 2009, **34**, 3.